Highly synergistic antimicrobial activity of spherical and flower-like hierarchical titanium dioxide/silver composites

Ye, Junwei; Cheng, Hang; Li, Hong; Yang, Yaoyao; Zhang, Siqi; Rauf, Nazifa Abdul

Published in:
Journal of Colloid and Interface Science

DOI:
10.1016/j.jcis.2017.05.111

Publication date:
2017

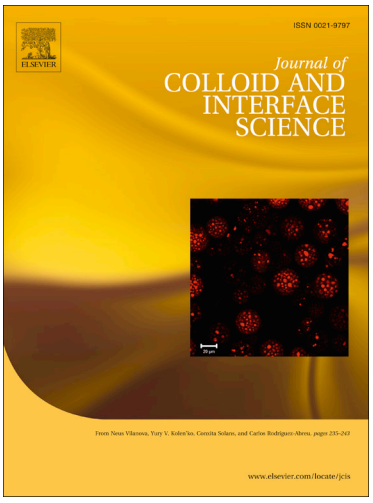

Highly synergistic antimicrobial activity of spherical and flower-like hierarchical titanium dioxide/silver composites

Junwei Ye, Hang Cheng, Hong Li, Yaoyao Yang, Siqi Zhang, Abdul Rauf, Qi Zhao, Guiling Ning

PII: S0021-9797(17)30647-1
DOI: http://dx.doi.org/10.1016/j.jcis.2017.05.111
Reference: YJCIS 22418

To appear in: *Journal of Colloid and Interface Science*

Received Date: 22 March 2017
Revised Date: 27 May 2017
Accepted Date: 29 May 2017

Please cite this article as: J. Ye, H. Cheng, H. Li, Y. Yang, S. Zhang, A. Rauf, Q. Zhao, G. Ning, Highly synergistic antimicrobial activity of spherical and flower-like hierarchical titanium dioxide/silver composites, *Journal of Colloid and Interface Science* (2017), doi: http://dx.doi.org/10.1016/j.jcis.2017.05.111

Highly synergistic antimicrobial activity of spherical and flower-like hierarchical titanium dioxide/silver composites

Junwei Ye,[a] Hang Cheng,[a] Hong Li,[b] Yaoyao Yang,[a] Siqi Zhang,[a] Abdul Rauf,[a] Qi Zhao,[*,c] Guiling Ning[*,a]

[a] *State Key Laboratory of Fine Chemicals and School of Chemical Engineering, Dalian University of Technology, 2 Linggong Road, Dalian 116024, P. R. China*

[b] *Liaoning Province Academy of Analytic Sciences, Standard System Engineering Research Center of Liaoning Province，Shenyang 110015, China*

[c] *Department of Mechanical Engineering, University of Dundee, DD1 4HN, UK*

ABSTRACT:

A spherical titanium dioxide/silver (TiO_2/Ag) composite and a flower-like hierarchical TiO_2/Ag composite were prepared *via* a template-induced method and a solvothermal method based on the Ag/Carbon spheres templates followed by calcination treatment, respectively. The morphologies of the composites were controlled by changing the concentration of reactants and calcination temperature. The antibacterial efficiency of the composites was evaluated with both Gram-negative *Escherichia coli* and Gram-positive *Staphylococcus aureus*, respectively. The minimal inhibitory concentration, morphological evolution of bacteria and fluorescent-based cell wall/membrane integrity were assayed. The synergistic effects of reactive oxygen

[*]Corresponding author. Tel.: +86 411 84986067; Fax: +86 411 84986065. E-mail address: ninggl@dlut.edu.cn (G. L. Ning); Q.Zhao@dundee.ac.uk (Q. Zhao).

species (ROS) and silver ions were observed, which lead to superior antibacterial activities of these TiO_2/Ag composites with a bacteriostatic rate as high as 99% even in the absence of light. The morphological effect of the composites on the antibacterial efficacy was also investigated. In addition, a durable antimicrobial coating was also fabricated by incorporating the hierarchical TiO_2/Ag composite into a commercial emulsion solution of polyvinyl acetate, which exhibited a promising application in bacterial sensitive locations.

Keywords: TiO_2/Ag composites; Antimicrobial; Sphere; Hierarchical structure; Coating

1. Introduction

Development of potent antibacterial materials has attracted tremendous attention from both the academic and industrial researchers due to the outbreak of infectious diseases caused by certain microorganisms, such as pathogenic *Escherichia coli* O-157, severe acute respiratory infection syndrome (SARS) and avian influenza virus [1, 2]. More severely, the emergence of antibiotic-resistant bacterial strains is considered as a serious global health issue [3]. Among various antibacterial materials, titanium dioxide (TiO_2) is a promising antibacterial agent due to its low cost, good chemical stability and environmentally friendly [4, 5]. It is well known that the

generation of destructive reactive oxygen species (ROS) under UV light irradiation plays the most important role for antibacterial efficacy of TiO_2, which may produce oxidative stress and attack bacterial cell, ultimately leading to the modification of membrane permeability and cell damaging [6, 7]. However, the relatively low antibacterial efficiency of pure TiO_2 in absence of UV or solar light irradiation greatly restricts its practical antimicrobial application.

Many attempts have been carried out to synthesize the TiO_2/metals (e.g. Cu [8], Zn [9], Ag [10] and Fe [11]) and TiO_2/non-metals composites [12-14], so as to efficiently extend their utility as biomedical materials. Among these composites, TiO_2/Ag composites are more potent antibacterial agents due to the fact that Ag nanoparticles (Ag NPs) deposited in TiO_2 matrix act as a conductor and charge separators for blocking electron-hole recombination, resulting in maximizing the production of ROS [15-17]. Furthermore, Ag NPs have been known as effective antimicrobial agents with broad-spectrum antibacterial activity, good durability, heat resistance and stability [18,19]. Recently, TiO_2/Ag composites with different morphologies were prepared by a range of various methods, including UV-irradiation, [16] solvothermal, [20] sol-gel, [21] and chemical deposition [22]. For example, Liu *et. al.* prepared TiO_2/Ag nanobelt by an alkaline hydrothermal method [23]. Chu *et. al.* prepared TiO_2/Ag tubes by an immersion method [24]. However, the controlled synthesis of TiO_2/Ag composites with tailored morphologies is still a great challenge [25-28].

In this paper, the spherical and flower-like hierarchical TiO_2/Ag composites were prepared by Ag/Carbon spheres as templates (Scheme 1). As expected, the

as-prepared composites show potent antimicrobial effects on both Gram-negative *Escherichia coli* (*E. coli*) and Gram-positive *Staphylococcus aureus* (*S. aureus*) in both dark and light. The synergistic antibacterial mechanism of the composites was proposed on the basis of the identification of the chemical origins and morphological changes of the bacteria. In addition, an eco-friendly antibacterial coating was also fabricated by incorporating TiO_2/Ag composites into commercial emulsion solutions of polyvinyl acetate (PVA).

2. Experimental

2.1. Synthesis of TiO_2/Ag composites

Titanium oxide (P25), silver nitrate ($AgNO_3$), glucose, hexadecyl trimethyl ammonium bromide (CTAB) and tetrabutyl titanate (TBT) were purchased from Sinopharm Chemical Reagent Co., Ltd. The Ag/Carbon spheres were synthesized by a solvethermal method [29]. 0.10 g CTAB and 0.20 g $AgNO_3$ were dissolved in 30 mL H_2O with the assistance of ultrasonication for 10 min. The mixture was added into a 40 mL glucose (5.00 g) aqueous solution with magnetic stirring for about 30 min. The mixture solution was transferred into a 100 mL autoclave with a Teflon seal and maintained at 180 °C for 16 h. After cooled to room temperature, black Ag/Carbon spheres were obtained.

To obtain the spherical TiO_2/Ag composite, the Ag/Carbon spheres were firstly dispersed in the absolute ethyl alcohol followed by addition of tetrabutyl titanate (TBT). A mixture of ethyl alcohol, acetic acid and distilled water was slowly dropped

into the above solution with vigorous stirring at room temperature. The precursor was collected by centrifugation and washed with absolute ethanol several times, and then was calcinated at determined temperature (450, 650 or 850 °C) under the N_2 atmosphere for 2 hours to obtain the spherical TiO_2/Ag composite.

To obtain the flower-like hierarchical TiO_2/Ag composite, the obtained Ag/Carbon spheres were dispersed in acetic acid followed by dropwise adding tetrabutyl titanate (TBT) with continuous stirring. The mixture solution was poured into a Teflon-lined autoclave and kept at 180 ℃ for 24 h. After cooled to room temperature, the precursor was collected by centrifugation, and then calcinated under the N_2 atmosphere to produce the flower-like hierarchical TiO_2/Ag composite.

2.2. Preparation of TiO_2/Ag composite coating

The coating was fabricated by incorporating hierarchical TiO_2/Ag composite into commercial emulsion solutions of polyvinyl acetate (PVA) under rapid stirring at 1500 rpm on a high-speed disperser at room temperature for 2 h. After being dried at 40 °C for 30 min, the TiO_2/Ag composite coating was obtained. As a control, the PVA coating and PVA/Ag NPs were also synthesized with the similar process, respectively.

2.3 Characterizations

X-ray powder diffraction (XRD, Rigaku-DMax 2400) with a 2θ scan configuration in the range 5–80° in reflection mode (Cu-Ka radiation) was used to characterize the TiO_2/Ag composites. Scanning electron microscope (SEM, Quanta-450, operated at 20 kV), field emission scanning electron microscope (FESEM, NOVA NANOSEM 450, measured at 15 kV) and energy dispersive X-ray

(EDX, Quanta-450 instrument) were operated to check the size and morphologies of samples. The X-ray photoelectron spectroscopy (XPS, ESCALAB250) was employed to study the surface atomic composition and chemical state. The adsorption–desorption isotherms of the composites was performed on An ASAP 2020 physical absorption apparatus. The optical density (OD) and photocatalytic properties were measured by a cell density meter (CO8000) and UV-vis diffuse reflectance spectroscope (UV-550). Fluorescent-Based cell wall/membrane integrity assay was carried out with fluorescence microscopy (OLYMPUS BX51). The fluorescence spectroscope was operated on FP-8300 Fluorescence Spectrometer. A xenon arc lamp (BL-GHX-IV, operated at 300 W) was used to provide simulated solar irradiation. Inductively coupled plasma atomic emission spectrometer (ICP-AES, Optima 200 DV, made by Perkin Elmer Company) was adopted to measure the silver content.

2.4. Antibacterial test

In order to evaluate the antimicrobial activities of the samples, the minimal inhibitory concentration (MIC), growth curves of bacteria and zone of inhibition against *E. coli* and *S. aureus* were investigated. All handlings of bacterial routine were operated with Luria Bertani (LB) broth at 37 °C. The medium was made up of dissolving agar and LB broth in distilled water. The sample was dispersed into sterilized tubes with 10 mL of liquid LB broth medium firstly. Then 50 μL of well cultivated bacterial solution (10^6 CFU mL^{-1}) was added to each tube. One group (three tubes) was put in the dark, while another was placed under the xenon arc lamp. After 30 min, 50 μL of supernatant was extracted from each tube and was uniformly spread

over several well solidified agar nutrient plates. After the incubation for 24 h, the colonies were counted and the percentage of inhibition of bacterial growth was evaluated using the following equation: $K = (N_{control} - N_{sample})/N_{control} \times 100\%$, where, K is the percentage of inhibition, $N_{control}$ is the colony forming units of control and N_{sample} is the CFU of various samples. The growth curve of bacteria were determined by using a cell density meter and the UV-Vis spectroscopy at 600 nm. Antibacterial activity of the Ag NPs and TiO_2 were also carried out using the same method as above.

To observe the morphological changes of bacterial cells after exposure to TiO_2/Ag composites, FESEM images were taken through the following procedures: the bacterial cultures containing *E. coli* or *S. aureus* and the composites were centrifuged and then washed twice with phosphate buffer saline followed by fixing with 2.5% glutaraldehyde solution for 4 h. The cells were dehydrated with sequential treatment of 50, 70, 80, 90, and 100% ethanol, respectively. After coated with gold by sputtering under vacuum, FESEM was operated. The numbers of live and dead bacteria were analyzed by a fluorescence staining method. Previous study [30,31] demonstrated that the acridine orange (AO) is cell-permeable and could stain the viable cells to green, while propidium iodide (PI) only stained the necrotic cells to red.

3. Result and discussion

3.1. Synthesis and Characterization of TiO_2/Ag composites

Spherical and flower-like hierarchical TiO_2/Ag composites were successfully synthesized by using Ag/Carbon sphere as templates (Scheme 1). Fig. S1 illustrates that the as-prepared Ag/Carbon spheres have uniform morphologies, with the diameter of about 500 nm. Fig. 1 shows the XRD patterns of as-prepared TiO_2/Ag composites. The characteristic diffraction peaks at 38.2, 44.3, 64.5 and 78.3º corresponding to (111), (200), (220) and (311) crystal planes, respectively, can be indexed as face-centred cubic (FCC) silver (JCPDS standard card No. 04-0783). Another peaks are in good agreement with the standard structure of titanium dioxide (JCPDS standard card No. 21-1272), while the diffraction peaks of the TiO_2 (004) crystal plane and the Ag (111) plane overlap each other because they are very adjacent.

The typical SEM and TEM images of both spherical and hierarchical TiO_2/Ag composites are shown in Fig. 2. In spite of the hollow interior of spherical TiO_2/Ag hybrid composite, it still retains the morphology of Ag/Carbon sphere with the diameter of about 400 nm (Figs. 2a and 2b). The related SEAD image (Fig. 2c) of hollow spherical TiO_2/Ag composite identifies the anatase phases of TiO_2 with characteristic diffraction ring of 101 crystal plane of TiO_2. As shown in Fig. 2e and 2f, the hierarchical TiO_2/Ag composite with diameter of 4-5 μm consists of many nano-needle units, and HRTEM image (Fig. 2g) reveals the typical lattice fringes of the both Ag and TiO_2, which are assigned to 0.235 nm of (111) plane of Ag and 0.352 nm of the (101) plane of TiO_2, respectively. The silver content in the TiO_2/Ag composite measured by EDX analysis is presented in Table S1. The measured silver

contents in the products were found to match well with the theoretical values. The peaks in the EDX spectra of both composites (Figs. 2d and 2h) corresponded to oxygen, silver, and titanium, respectively, and no other impurities were detected.

To further confirm the elemental presence status in the composites, the X-ray photoelectron spectroscopy (XPS) analysis was carried out. As shown in Fig. 3, the peaks matched with Ag (3d), Ti (3p, 3s, 2p, 2s) and O (2p, 2s, 1s) were detected, respectively. Fig. 3b also displays the high energy resolution XPS spectrum of Ag 3d region. Both the peaks at 367.6 and 373.6 eV demonstrated that the silver is Ag^0 metallic state. The slitting of the 2p doublet of Ti indicates the normal state of Ti^{4+} in the composites. Each peak can also be deconstructed into two Gaussian components with identical full width at half maximum parameter. The deconstructed peak at 458.1 eV matches well with the presence of Ti^{3+}, which can arise from the incorporation of silver on the matrix of TiO_2 [32].

Fig. 4 presents the N_2 adsorption-desorption isotherms of the commercial TiO_2 (P25), spherical and hierarchical TiO_2/Ag composites. The Brunauer-Emmett-Teller (BET) surface area of the hierarchical composite is 188.59 m^2/g, which is higher than that of spherical composite (108.36 m^2/g) and P25 (42.11 m^2/g). Both the spherical composite and commercial P25 show the type II isotherm with type H3 hysteresis loops, while the hierarchical TiO_2/Ag composite exhibits the type III isotherm with type H3 hysteresis loop, which are the typical characteristics of mesoporous and macroporous materials.

3.2. Effect of reactant concentration and calcination temperature

The effect of reactant concentration on the structures of TiO_2/Ag composites was investigated. When the molar composition of Ti/Ag was 100 or 75, all the diffraction peaks matched well with the anatase TiO_2 (JCPDS standard card No. 21-1272) (Fig. S2). In addition, the XRD patterns did not show obvious diffraction peaks corresponding to silver species as they might be too less to be detected. The characteristic diffraction peaks of Ag crystal plane appeared while the molar composition of Ti/Ag reduced from 50 to 25. The intensities of peaks of the Ag crystal planes gradually became stronger with the increase of Ag^+ concentration, indicating that the Ag nanocrystals were growing with the increasing concentration of silver ions. In addition, the average size of Ag nanocrystals, measured by using the Debye–Scherrer equation based on the full width at half-maximum of the diffraction peak were 12.8, 19.7, and 24.7 nm, respectively. In the FT-IR (Fig. S3), the peaks around 3430, 1630 and 1380 cm^{-1} could be attributed to the O-H stretching vibration and O-H bending of water molecules adsorbed onto the surface of the particles [33], respectively. The broad band around 680 cm^{-1} observed was associated with TiO_2 crystal lattice vibrations [34, 35].

Fig. 5 illustrates the SEM images of hierarchical TiO_2/Ag composite with different molar composition of Ti/Ag. When the Ti/Ag molar ratio was 25, the micron-sized hierarchical composites with diameter of about 400 nm were synthesized. However, the submicron-sized ellipsoid spheres were obtained as the molar ratio increased from 50 to 100. To identify the effect of calcination temperature, the precursors were sintered at different temperature (450, 650 or 850 °C) under the

N_2 atmosphere for 2 hours and then in static air for 2 h to obtain the TiO_2/Ag composites. While the temperature increased from 450 °C to 850 °C, the intensities of the rutile peaks rise in comparison to anatase peaks (Fig. S4). When sample was calcined at 650 °C, XRD pattern indicated that the mixture of anatase and rutile TiO_2 was obtained, caused by generated more oxygen vacancies by doping silver ions into TiO_2 [36]. When the temperature was up to 850 °C, the product was entirely in the rutile phase. Noticeably, the characteristic peaks of samples tended to shift slightly to lower degree compared to that of pure TiO_2, which may also be due to a small amount of silver ions doped into TiO_2 at higher annealing temperature.

3.3. Antibacterial activity of TiO_2/Ag composites

The OD_{600} curves (Fig. 6) show that the minimal inhibition concentrations (MICs) of hierarchical TiO_2/Ag composites against both *E. coli* and *S. aureus* were in the range of 50-100 ppm. However, MICs of spherical TiO_2/Ag composite were about 200 ppm, while that of the pure Ag NPs and commercial TiO_2 (P25) were greater than 500 ppm. Fig. 7 shows the bacterial reduction assay of TiO_2/Ag composites. The percentages of inhibition for P25, Ag NPs, spherical and hierarchical TiO_2/Ag composites towards *E. coli* were 39%, 62%, 99% and 99%, respectively. Similarly, for *S. aureus*, they were 31%, 53%, 92% and 99%, respectively. *S. aureus* seems to be less susceptible than *E. coli*, which would be due to the cell wall of Gram-positive bacteria is thicker than that of Gram-negative. The bacterial reduction assays of *E. coli* and *S. aureus* treated by commercial P25, Ag NPs, spherical and hierarchical

TiO_2/Ag composites in the dark were also carried out (Fig. S5). It can be seen that all composites showed the superior antibacterial activity than that of P25 and Ag NPs.

The fluorescence microscope is another effective approach to observe bacterial inactivation process. Fig. 8 shows the fluorescence images of bacteria after exposure to hierarchical TiO_2/Ag composite with different time. At the beginning, almost all of the bacteria showed green (Figs. 8a and 8d), which demonstrates that bacteria were viable. However, a lot of *E. coli* and *S. aureus* were stained red after treatment for 2 h (Figs. 8b and 8e), while nearly all the bacteria were stained red after treatment for 24 h (Figs. 8c and 8f), indicating that this composite had strong damaging effect on the cell membrane and made the cell loss viability.

3.4. Synergistic antibacterial mechanism of TiO_2/Ag composites

Previous studies suggested that the antibacterial activities of TiO_2-based materials were attributed to photocatalytic activity for generating reactive oxygen species (ROS), such as •OH radicals [37]. These ROS may produce oxidative stress and then attack membrane lipids, ultimately leading to membrane or DNA damage. Comparing to that of commercial TiO_2, the broader UV-vis absorption spectra of both as-prepared spherical and hierarchical TiO_2/Ag composites showed a better light utilization rate toward the visible region (Fig. S6). This may be attributed to the surface plasmon absorption effect of Ag NPs deposited on the surface of composites [38], which would strengthen their antibiotic capability. Fluorescence method with terephthalic acid (TA) as the probe was employed for the quantification of ·OH radicals [39,40]. The unique fluorescence signal peaked at 426 nm were observed (Fig. 9). The mixture solution of

terephthalic acid (TA) and hierarchical Ag/TiO_2 composites showed the strongest fluorescent intensity, than other solutions containing TA and spherical composite, commercial P25 and Ag NPs, respectively. This result indicated that antibacterial efficiency of hierarchical Ag/TiO_2 was the highest among these agents which was consistent with the bacterial reduction assays.

It is well known that the silver ions tend to interact with cell membrane/wall of bacteria [41] leading to the death of these bacteria. The ICP-AES was used to determine the Ag^+ ion release ability of both spherical and hierarchical TiO_2/Ag composites. After 24 h, the concentrations of Ag^+ ions released from spherical and hierarchical TiO_2/Ag composites were 0.625 ppm and 0.583 ppm, respectively, which were slightly higher than that released from Ag NPs (0.330 ppm). Noticeably, the intensities of fluorescence signals generated by the mixture solution of TA and composites were almost the same in the dark (Fig. S7) meaning the Ag^+ ions actually affected bactericidal effect in dark dominantly. Ag NPs incorporated into TiO_2 did not lose their antimicrobial properties.

Furthermore, SEM analysis was employed to investigate the surface morphology changes of bacteria. The intact *E. coli* and *S. aureus* have distinct outer membranes (Figs. 10a and 10d). After treatment with hierarchical TiO_2/Ag composite for 2 h, the morphologies of a portion of *E. coli* and *S. aureus* significantly changed (Figs. 10b and e). When bacteria were exposed to the composites for 24 h, the cellular cohesion was weaken with the seriously damage of the outer membranes (Figs. 10c and f) and cytoplasm was flowed out, resulting in the death of bacteria. Fig. 11 shows the high

resolution TEM images of *E. coli* treated with spherical and hierarchical TiO_2/Ag composites, respectively. Compared with isotropy of spherical composite (Fig 11a), the hierarchical composite with nano-needle units had bigger effective target area (Fig 11b) and stronger penetration capability towards bacteria, which caused seriously damage of the cell membranes [42].

Based on above-mentioned analysis, the synergistic antibacterial mechanism of TiO_2/Ag composites was proposed as followings: i) Ag NPs decorated on TiO_2 enhance generation of destructive ROS; ii) Ag^+ ions released continuously from composites lead to the death of bacteria in both the light and the dark; iii) the higher BET surface area and nanoneedle struture can enhance antimicrobial properties. Finally, as-prepared TiO_2/Ag composites showed potent antibacterial behavior.

3.5. Antibacterial activities of coating

Coating with good antibacterial properties is desirable for practical applications. An antibacterial coating was also prepared by incorporating as-prepared TiO_2/Ag composites into commercial emulsion solutions of polyvinyl acetate (PVA). The antibacterial activities of the TiO_2/Ag/PVA against *E. coli* and *S. aureus* were investigated, respectively, by inhibition zone test. As shown in Fig. 12, the pure PVA coating displays no obvious inhibition zone. The PVA coatings modified with the commercial P25 and Ag NPs appeared inhibition function on the growth of bacteria. Comparing to above coatings, the TiO_2/Ag/PVA coating shows the good inhibition zone. These results indicated TiO_2/Ag/PVA coating is a promising antimicrobial material in potential application.

4. Conclusion

In summary, the spherical and flower-like hierarchical TiO_2/Ag composites were successfully prepared by a template-induced method and a solvothermal method using Ag/Carbon spheres as precursor, respectively. The as-prepared spherical TiO_2/Ag composite remains the morphologies of Ag/Carbon spheres with the diameter of about 400 nm, whereas the hierarchical TiO_2/Ag composite with diameter of 4-5 μm was consists of many nano-needle units. Both the spherical and hierarchical TiO_2/Ag composites possessed high Brunauer-Emmett-Teller (BET) surface area, which were 108.36 and 188.59 $m^2 \cdot g^{-1}$, respectively. They exhibited the enhanced antibacterial activities against *E. coli* and *S. aureus* not only in the presence of light but also in the dark. The minimal inhibition concentrations of spherical and hierarchical TiO_2/Ag composites against *E. coli* and *S. aureus* were in the range of 200-250 and 50-100 μg/mL, respectively. The synergistic antibacterial effect of both Ag NPs and TiO_2 was based on the generation of ROS and release of silver ions. In addition, composites damaged the cell membrane with the loss of cell viability. The enhanced antibacterial ability of TiO_2/Ag composites was superior to that of commercial TiO_2 and Ag NPS under identical conditions. Moreover, the eco-friendly TiO_2/Ag/polyvinyl acetate coating was also fabricated, and it displayed a promising application as an antibacterial materials. The work may offer insights for developing facile methods to prepare composites and understanding of synergistically antibacterial mechanism of multi-component antibacterial agents.

Supporting Information

SEM images, XRD, FT-IR spectra, optical images, fluorescence spectra and silver content. The supporting information is available free of charge.

Note

The authors declare no competing financial interest.

ACKNOWLEDGMENTS

The authors acknowledge financial supported from the National Natural Science Foundation of China (U1607101 and 21476045) and Natural Science Foundation of Liaoning Province (2015020199). We thank Dr. Wenjie Yuan for many helpful suggestions to antibacterial experiments.

REFERENCES

[1] M. Gomółka-Pawlicka, J. Uradziński, A. Migowska-Calik, M. Pastuszczak-Frąk, African J. Microbio. Res. 7 (2013) 361-366.

[2] Z. Zhao, F. Zhang, M. Xu, K. Huang, W. Zhong, W. Cai, Z. Yin, S. Huang, Z. Deng, M. Wei, J. Xiong, P. M. Hawkey, J. Med. Microbiol. 52 (2003) 715-720.

[3] J. López-Esparza, L. F. Espinosa-Cristóbal, A. Donohue-Cornejo, S. Y. Reyes-López, Ind. Eng. Chem. Res. 55 (2016) 12532−12538.

[4] M. Dahl, Y. Liu, Y. Yin, Chem. Rev. 114 (2014) 9853-9889.

[5] H. Bai, Z. Liu, L. Liu, D. D. Sun, Chem. Eur. J. 19 (2013) 3061-3070.

[6] S. Pigeot-Rémy, F. Simonet, E. Errazuriz-Cerda, J. C. Lazzaroni, D. Atlan, C. Guillard, Appl. Catal. B-Environ. 104 (2011) 390-398.

[7] R. A. Palominos, M. A. Mondaca, A. Giraldo, G. Peñuela, M. Pérez-Moya, H. D Mansilla, Catal. Today. 144 (2009) 100-105.

[8] S. Chen, Y. Guo, H. Zhong, S. Chen, J. Li, Z. Ge, J. Tang, Chem. Eng. J. 256 (2014) 238-246.

[9] S. H. Hwang, J. Song, Y. Jung, O. Y. Kweon, H. Song, J. Jang, Chem. Commun. 47 (2011) 9164-9166.

[10] J. Thiel, L. Pakstis, S. Buzby, M. Raffi, C. Ni, D.J. Pochan, S.I. Shah, Small 3 (2007) 799-803.

[11] S. Naghibi, S. Vahed, O. Torabi, A. Jamshidi, M. H. Golabgir, Appl. Sur. Sci. 327 (2015) 371-378.

[12] C. W. H. Dunnill, Z. A. Aiken, J. Pratten, M. Wilson, D. J. Morgan, I. P. Parkin, J. Photoch. Photobio. A: Chem. 207 (2009) 244-253.

[13] J. C. Yu, W. Ho, J. Yu, H. Yip, P. K. Wong, J. Zhao, Environ. Sci. Technol. 39 (2005) 1175-1179.

[14] X. Xue, Y. Wang, H. Yang, Appl. Sur. Sci. 264 (2013) 94-99.

[15] M. M. Khan, S. A. Ansari, M. I. Amal, J. Lee, M. H. Cho, Nanoscale. 5 (2013) 4427-4435.

[16] M. Li, M. E. Noriega-Trevino, N. Nino-Martinez, C. Marambio-Jones, J. Wang, R. Damoiseaux, F. Ruiz, E. M. Hoek, Environ. Sci. Technol. 45 (2011) 8989-8995.

[17] S. Wang, H. Qian, Y. Hu, W.Dai, Y. Zhong, J. Chen, X. Hu, Dalton Trans. 42 (2013) 1122-1128.

[18] A. B. Smetana, K. J. Klabunde, G. R. Marchin, C. M. Sorensen, Langmuir 24 (2008) 7457-7464.

[19] S. Eckhardt, P. S. Brunetto, J. Gagnon, M. Priebe, B. Giese, K. M. Fromm, Chem. Rev. 113 (2013) 4708-4754.

[20] C. Jia, P. Yang, J. Li, B. Huang, K. Matras-Postolek, ChemCatChem 8 (2016) 839-847.

[21] Y.F. Joya, Z. Liu, T. Wang, Appl. Phys. B. 105 (2011) 525-536.

[22] M. Es-Souni, M. Es-Souni, S. Habouti, N. Pfeiffer, A. Lahmar, M. Dietze, C. H. Solterbeck, Adv. Fun. Mater. 20 (2010) 377-385.

[23] J. Wang, W. Liu, H. Li, H. Wang, Z. Wang, W. Zhou, H. Liu, Chem. Eng. J. 228 (2013) 272-280.

[24] L. Zhao, H. Wang, K. Huo, L. Cui, W. Zhang, H. Ni, Y. Zhang, Z. Wu, P. K. Chu, Biomaterial 32 (2011) 5706-5716.

[25] G. Tian, Y. Chen, W. Zhou, K. Pan, C. Tian, X. Huang, H. Fu, CrystEngComm 13 (2011) 2994-3000.

[26] X. Lu, J. Ye, Y. Sun, R. F. Bogale, L. Zhao, P. Tian, G. Ning, Dalton Trans. 43 (2014) 10104–10113.

[27] H. Cheng, J. W. Ye, Y. Sun, W. J. Yuan, J. Y. Tian, R. F. Bogale, P. Tian, G. L. Ning, RSC Adv. 5 (2015) 80668–80676.

[28] Q. Zhang, J. W. Ye, P. Tian, X. Y. Lu, Y. Lin, Q. Zhao, G. L. Ning, RSC Adv. 3 (2013) 9739-9744.

[29] S. H. Yu, X. Cui, L. Li, K. Li, B. Yu, M. Antonietti, H. Coelfen, Adv. Mater. 16 (2004) 1636-1640.

[30] J. R. Nakkala, R. Mata, A. K.Gupta, S. R. Sadras, Eur. J. Med. Chem. 85 (2014) 784-794.

[31] K. Mascotti, J. McCullough, S. R. Burger, Transfusion (Paris), 40 (2000) 693-696.

[32] O. Akhavan, E. Ghaderi, Surf. Coat. Technol. 204 (2010) 3676-3683.

[33] T. Peng, D. Zhao, K. Dai, W. Shi, K. Hirao, J. Phys. Chem. B.109 (2005) 4947-4952.

[34] J.C. Yu, L. Zhang, Z. Zheng, J. Zhao, Chem. Mater. 15 (2003) 2280-2286.

[35] H. R. Pant, B. Pant, R. K. Sharma, A. Amarjargal, H. J. Kim, C. H. Park, L. D. Tijing, C. S. Kim, Ceram. Int. 39 (2013) 1503-1510.

[36] S. I. Mogal, V. G. Gandhi, M. Mishra, S. Tripathi, T. Shripathi, P.A. Joshi, D. O. Shah, Ind. Eng. Chem. Res. 53 (2014) 5749-5758.

[37] T. Tong, A. Shereef, J. Wu, C. T. Binh, J. J. Kelly, J. F. Gaillard, K. A. Gray, Environ. Sci. Technol. 47 (2013) 12486-12495.

[38] H. Tada, T. shida, A. Takao, S. Ito, Langmuir. 20 (2004) 7898-7900.

[39] J. Hu, Z. X. Zhong, F. Zhang, W. H. Xing, W. J. Jin, N. P. Xu , Ind. Eng. Chem. Res. 55 (2016) 6661−6670.

[40] G. Liu, P. Niu, L. Yin, H. M. Cheng, J. Am. Chem. Soc. 134 (2012) 9070-9073.

[41] M. Zhang, P. Wang, H. Sun, Z. Wang, ACS Appl. Mater. Inter. 6 (2014) 22108-22115.

[42] J. Feng, L.Y. Zou, Y. T. Wang, B. W. Li, X. F. He, Z. J. Fan, Y. Ren, Y. Z. Lv, M. L. Zhang, D. Chen, J. Colloid Inter. Sci. 438 (2015) 259-267.

Captions

Scheme 1. Schematic illustration for the synthesis of TiO_2/Ag composites.

Fig. 1. XRD patterns of spherical and hierarchical TiO_2/Ag composites.

Fig. 2. SEM (a), TEM (b) and SEAD (c) images of spherical TiO_2/Ag composite. SEM (d), TEM (e) and HRTEM (f) images of hierarchical TiO_2/Ag composite.

Fig. 3. Overall (a) and high-resolution (b) XPS spectra of spherical and hierarchical TiO_2/Ag composites.

Fig. 4. N_2 adsorption-desorption isotherms of the commercial P25, spherical and hierarchical TiO_2/Ag composites.

Fig. 5 SEM images of hierarchial TiO_2/Ag composites with different molar composition of Ti/Ag (a) 100, (b) 75, (c) 50, (d) 25.

Fig. 6 Bacterial growth curve of *E. coli* (a) and *S. aureus* (b) treated with commercial P25, Ag NPs, spherical and hierarchical TiO_2/Ag composites with different concentration.

Fig. 7. Optical images (a-j) and graph of percentage of inhibition against *E. coli* and *S. aureus*. (k) Percentage of inhibition for control experiment, P25, Ag NPs, spherical and hierarchical TiO_2/Ag composites towards *E. coli*.

Fig. 8. Fluorescent images of *E. coli.* (a-c) and *S. aureus.* (d-f) treated by hierarchical TiO_2/Ag composites with different time: (a, d) 0 h, (b, e) 2 h, and (c, f) 24 h.

Fig. 9. Fluorescence spectra of mixtures of TA with •OH radicals generated by the P25, Ag NPs, spherical and hierarchical TiO_2/Ag composites, respectively.

Fig. 10. SEM images of *E. coli* (a-c) and *S. aureus* (d-f) treated by hierarchical TiO_2/Ag composite with different time: (a and d) 0 h, (b and e) 2 h, and (c and f) 24 h.

Fig. 11. TEM images of *E. coli* treated with (a) spherical and (b) hierarchical TiO_2/Ag composites.

Fig. 12. Inhibition zone of different coatings against (a) *E. coli* and (b) *S. aureus*.

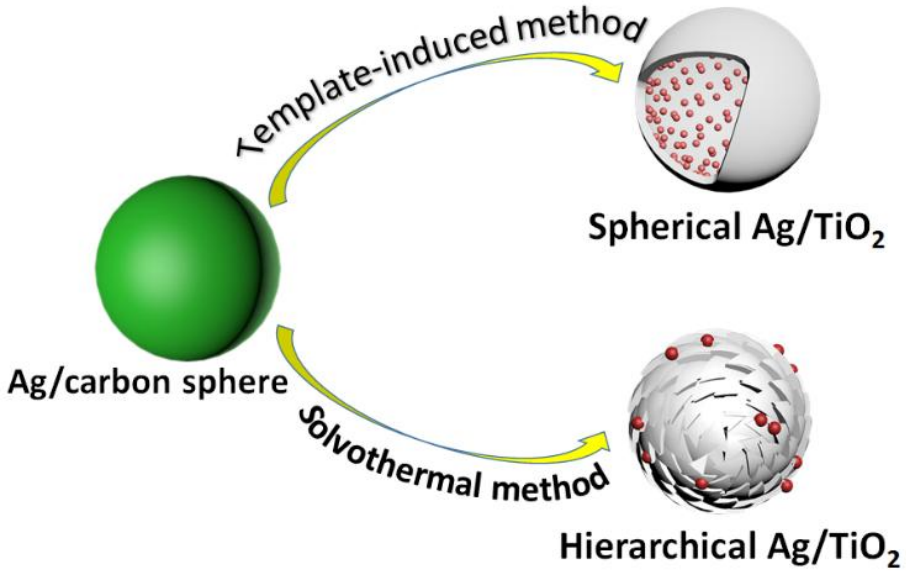

Scheme 1. Schematic illustration for the synthesis of TiO_2/Ag composites.

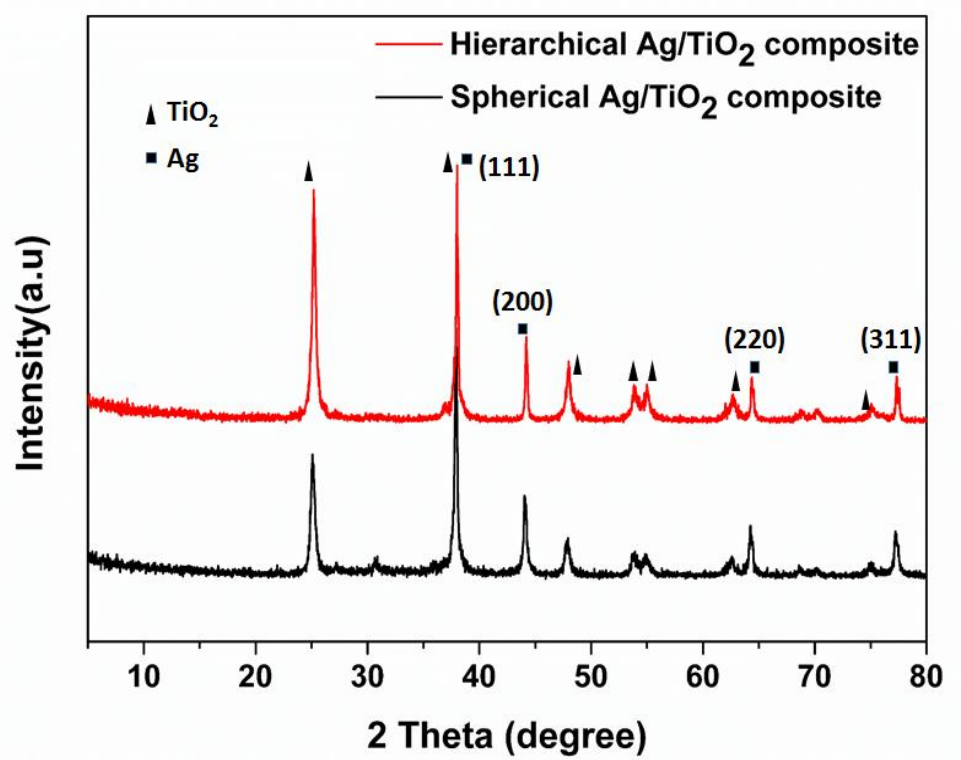

Fig. 1. XRD patterns of spherical and hierarchical TiO_2/Ag composites.

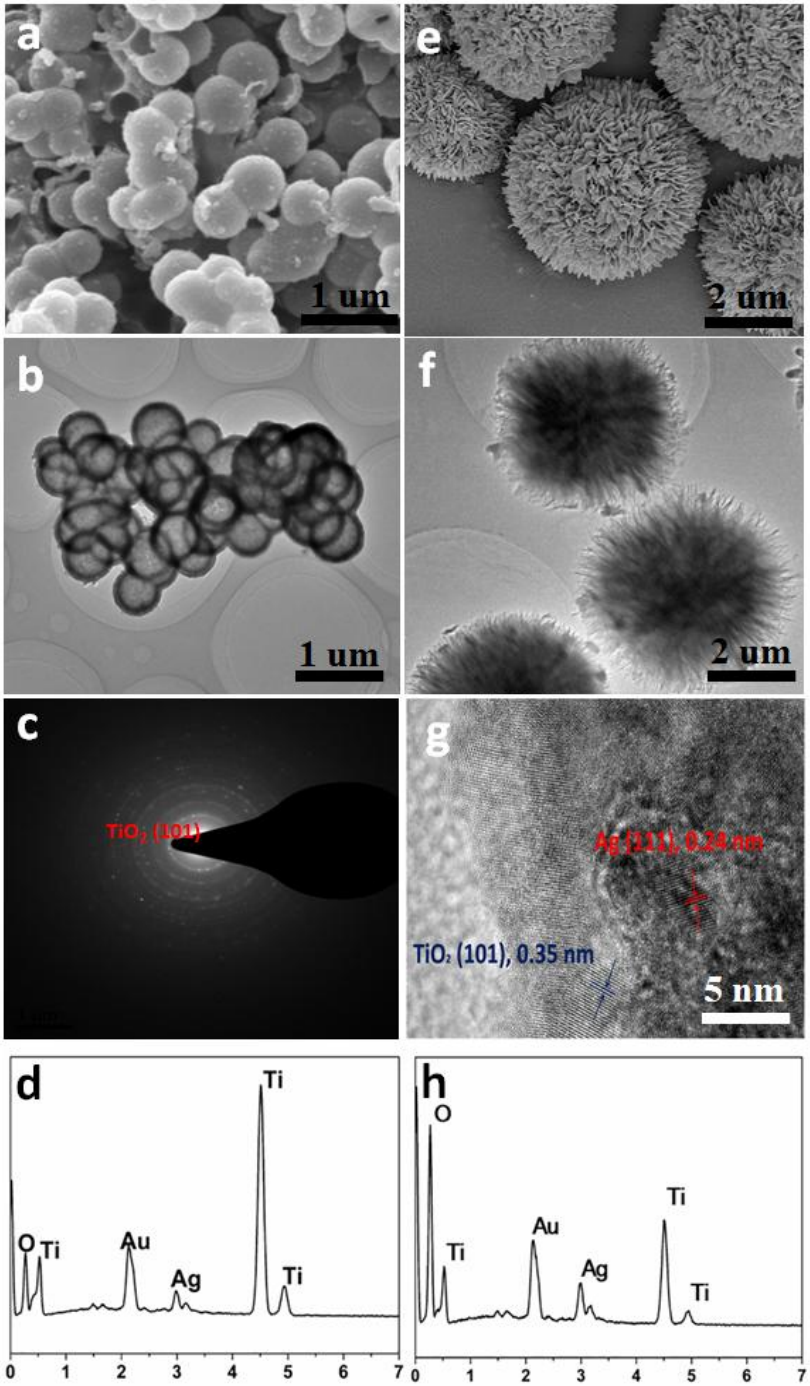

Fig. 2. SEM (a), TEM (b) and SEAD (c) and EDX (d) images of spherical TiO_2/Ag composite. SEM (e), TEM (f) and HRTEM (g) and EDX (h) images of hierarchical TiO_2/Ag composite.

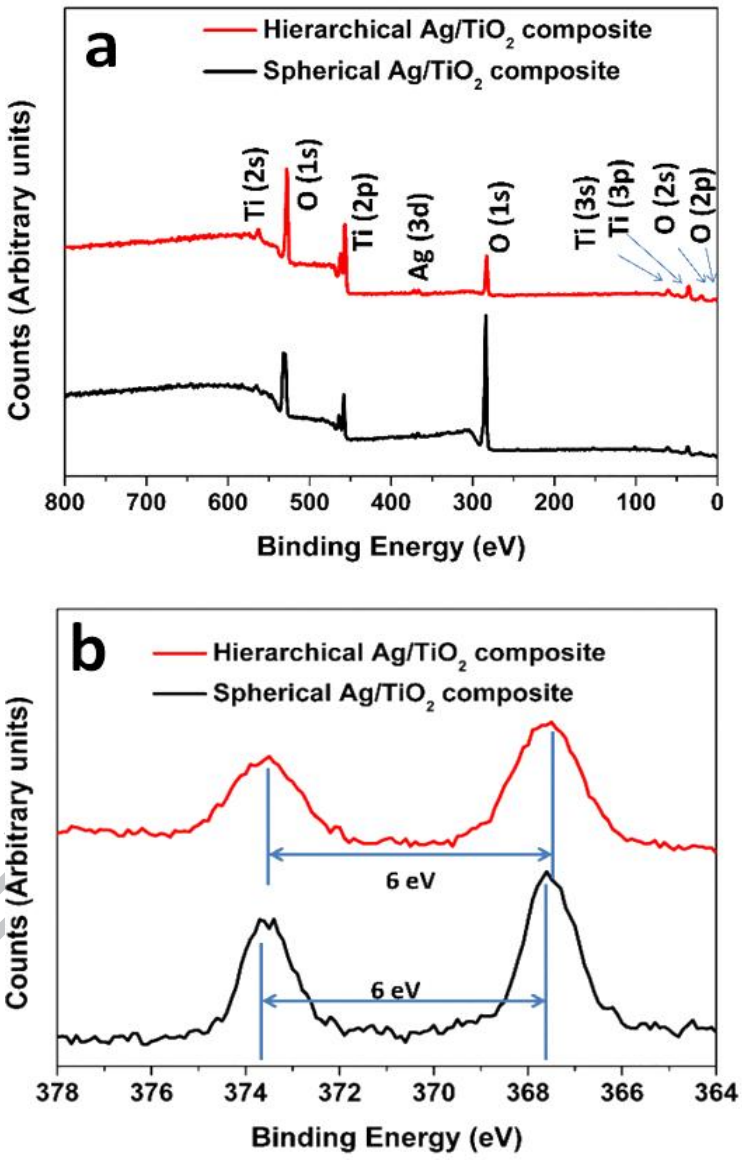

Fig. 3. Overall (a) and high-resolution (b) XPS spectra of spherical and hierarchical TiO_2/Ag composites.

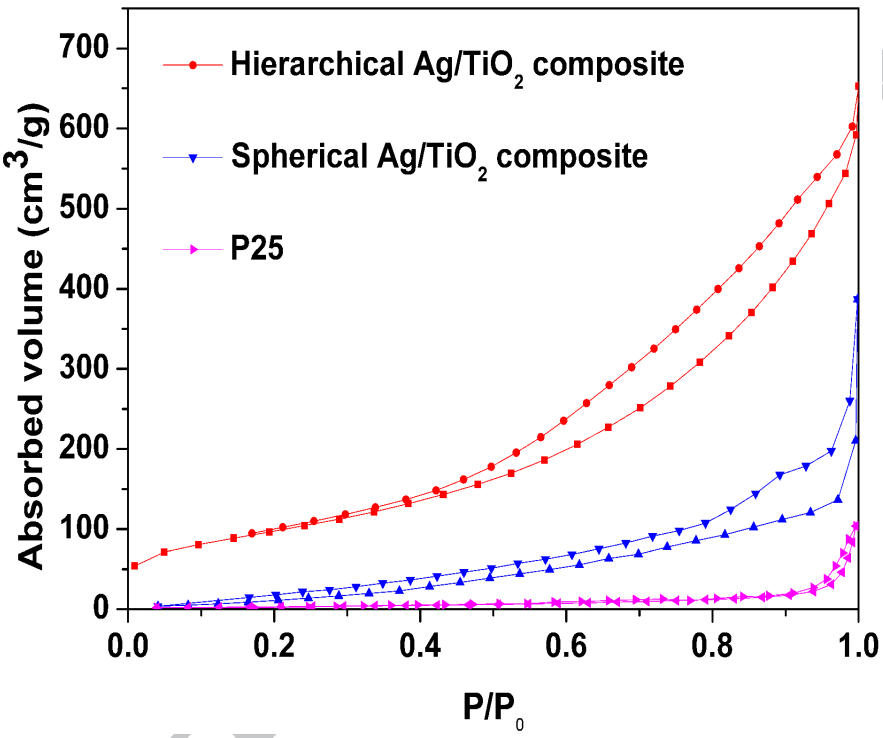

Fig. 4. N_2 adsorption-desorption isotherms of the commercial P25, spherical and hierarchical TiO_2/Ag composites.

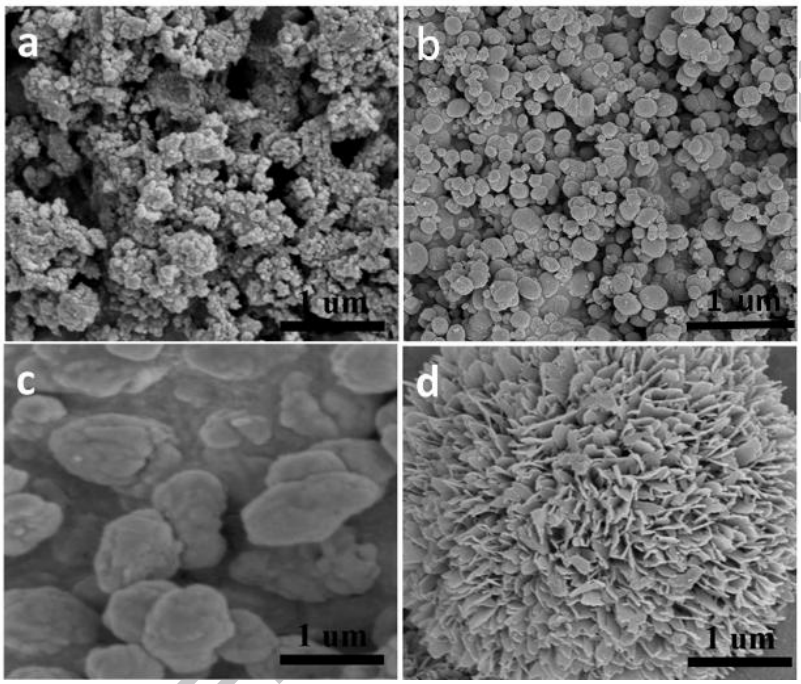

Fig. 5 SEM images of hierarchial TiO_2/Ag composites with different molar composition of Ti/Ag (a) 100, (b) 75, (c) 50, (d) 25.

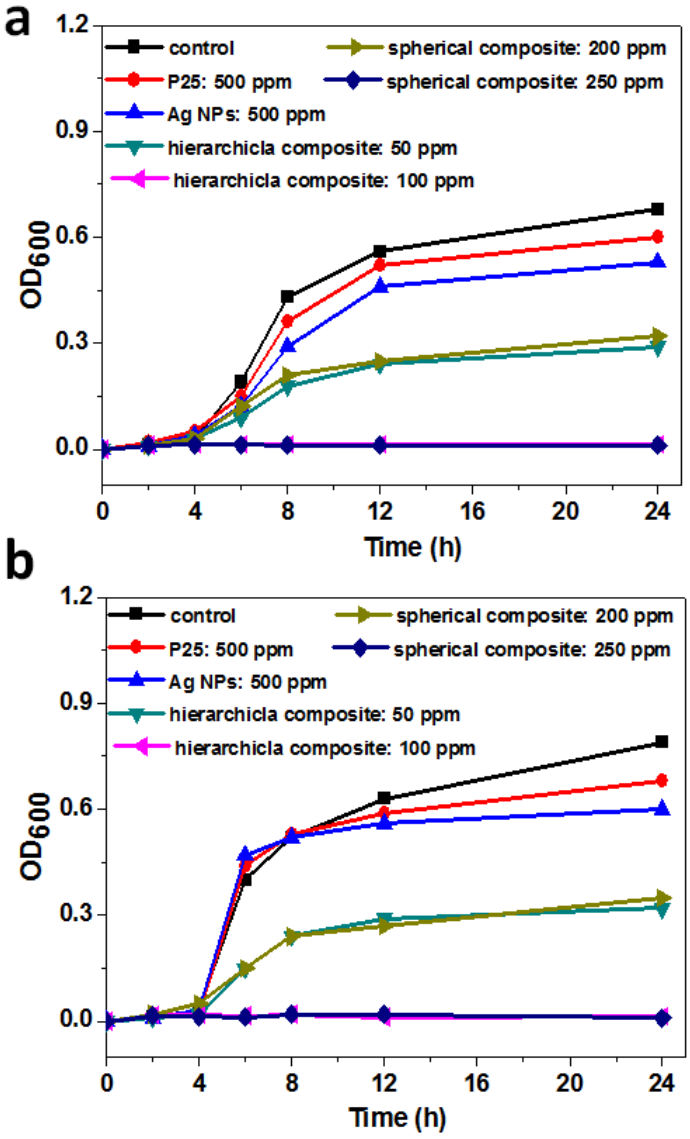

Fig. 6 Bacterial growth curve of *E. coli* (a) and *S. aureus* (b) treated with commercial P25, Ag NPs, spherical and hierarchical TiO_2/Ag composites with different concentration.

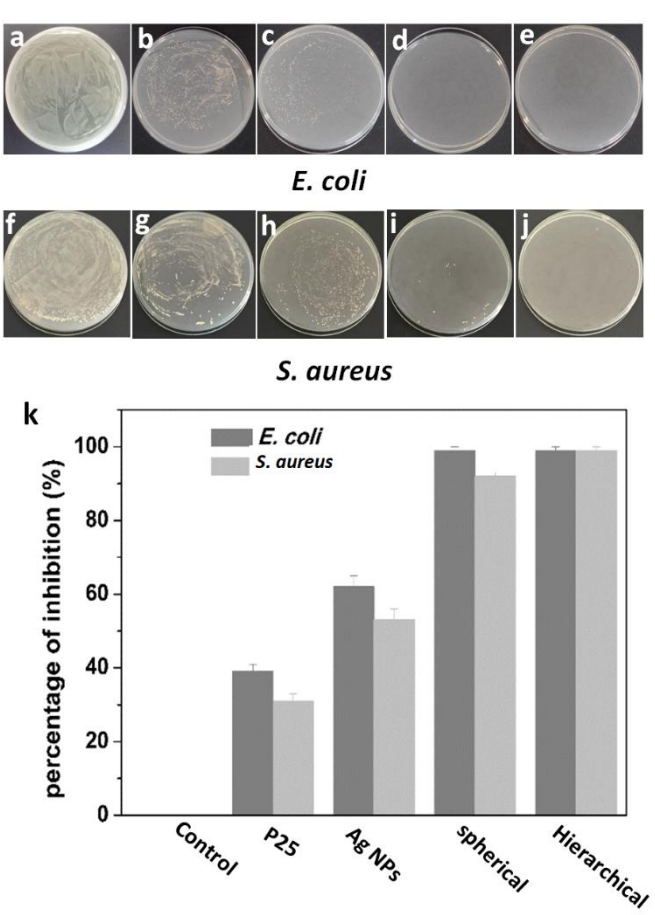

Fig. 7. Optical images (a-j) and graph of percentage of inhibition against *E. coli* and *S. aureus*. (k) Percentage of inhibition for control experiment, P25, Ag NPs, spherical and hierarchical TiO_2/Ag composites towards *E. coli*.

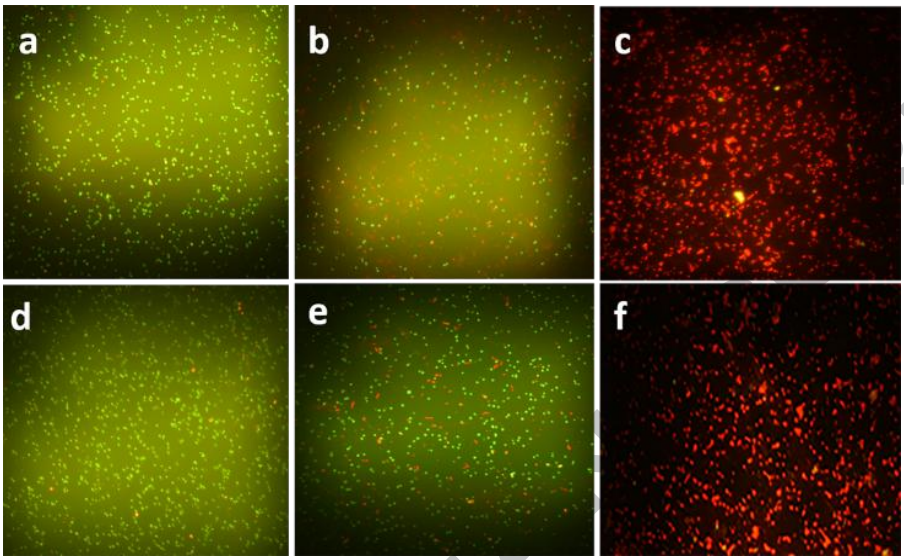

Fig. 8. Fluorescent images of *E. coli.* (a-c) and *S. aureus.* (d-f) treated by hierarchical TiO_2/Ag composites with different time: (a, d) 0 h, (b, e) 2 h, and (c, f) 24 h.

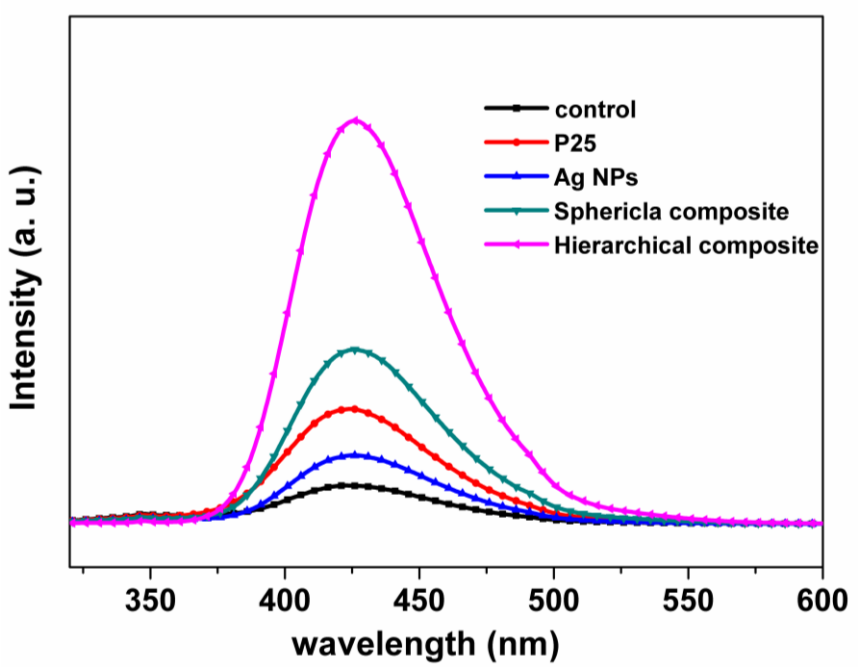

Fig. 9. Fluorescence spectra of mixtures of TA with •OH radicals generated by the P25, Ag NPs, spherical and hierarchical TiO_2/Ag composites, respectively.

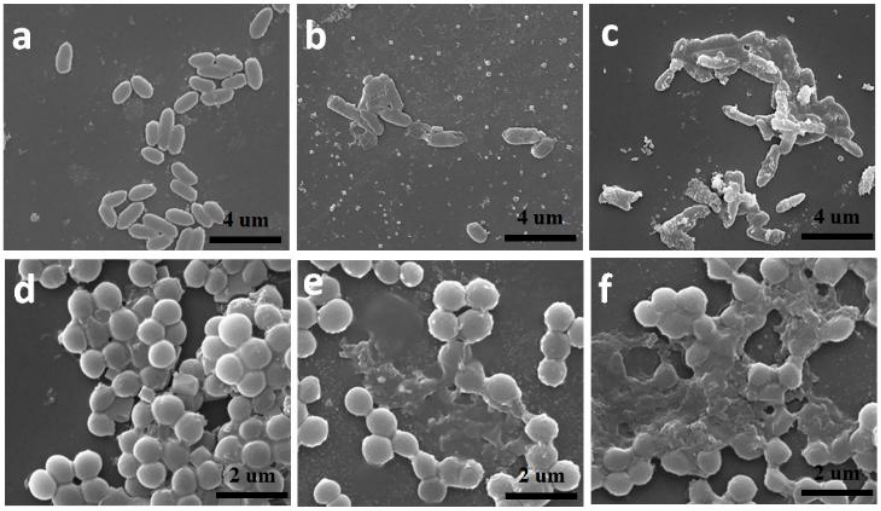

Fig. 10. SEM images of *E. coli* (a-c) and *S. aureus* (d-f) treated by hierarchical TiO_2/Ag composite with different time: (a and d) 0 h, (b and e) 2 h, and (c and f) 24 h.

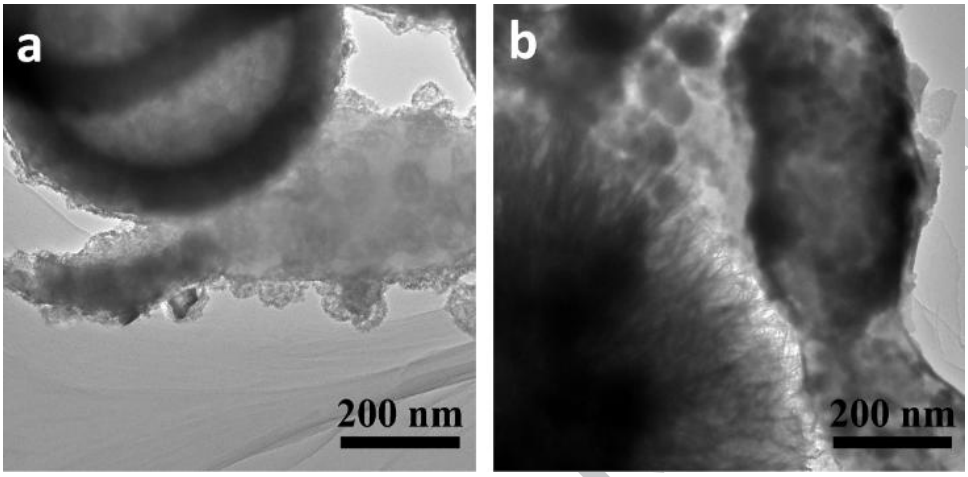

Fig. 11. TEM images of *E. coli* treated with (a) spherical and (b) hierarchical TiO_2/Ag composites.

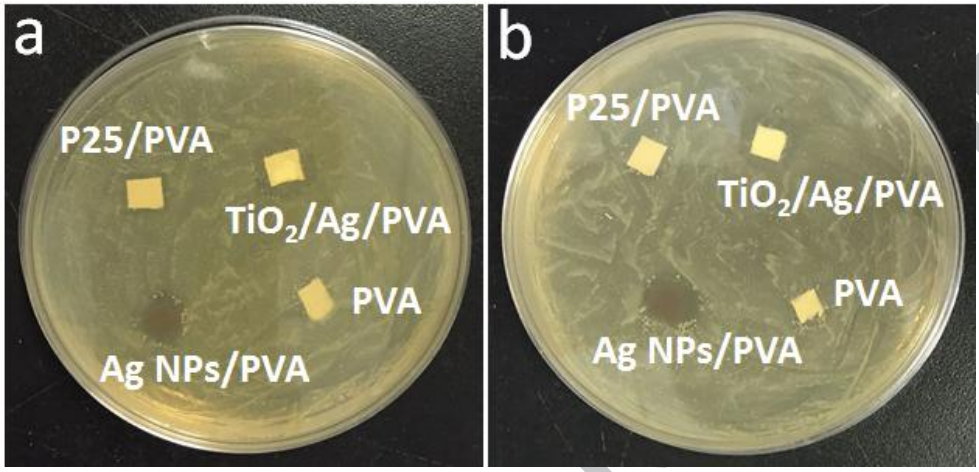

Fig. 12. Inhibition zone of different coatings against (a) *E. coli* and (b) *S. aureus*.

Graphical abstract

Spherical and hierarchical flower-like Ag/TiO_2 composites were synthesized by a facile Ag/carbon spheres-induced route and they show superior antimicrobial activities with a bacteriostatic rate as high as 99%.